J. Water Environ. Nanotechnol., 4(4): 275-284 Autumn 2019

ORIGINAL RESEARCH PAPER

Influence of membrane morphology on humic acid removal behavior of adsorptive membrane by embedding modified montmorillonite

***Elham Shokri*[1,*], *Reza Yegani*[2]**

[1] *Department of Chemical Engineering, University of Bonab, Bonab, Iran*
[2] *Faculty of Chemical Engineering, Sahand University of Technology, Tabriz, Iran*

Received: 2019-09-03 Accepted: 2019-10-26 Published: 2019-11-01

ABSTRACT

In this study, the efficiency of two different morphologies of polysulfone adsorptive membranes was examined for the humic acid removal from contaminated water. Adsorptive membranes with finger-like and sponge-like pore structures were prepared using modified montmorillonite with amino acid. The structure of fabricated membranes was investigated by Field Emission-Scanning Electron Microscopy, pure water flux, porosity and contact angle measurement. The obtained results showed that the addition of modified montmorillonite (MMT) to the membrane with finger-like structure altered the morphology and improved pure water flux, porosity, and hydrophilicity. These changes were negligible in PSf with sponge-like structure. In addition, the adsorption property of these membranes for the removal of humic acid (HA) was extensively studied. The adsorption capacity of cellular membrane was higher than the finger-like structure and Freundlich isotherm model was fitted for both of them. Nevertheless, the membrane with finger-like pores provides rapid adsorption of HA respect to cellular structure. It was also found that increasing the pH until pH=8 enhanced HA removal for adsorptive membranes, but increasing the pH above this point was not favorable. The obtained results from the dynamic adsorption revealed that sponge-like and finger-like membranes could generate 100 mL and 50 mL permeate of high quality (<1 ppm HA in water), respectively.

Keywords: *Adsorptive membrane, pore structure, humic acid, montmorillonite, amino acid*

How to cite this article
Shokri E, Yegani R. Influence of membrane morphology on humic acid removal behavior of adsorptive membrane by embedding modified montmorillonite. J. Water Environ. Nanotechnol., 2019; 4(4): 275-284. DOI: 10.22090/jwent.2019.04.002

INTRODUCTION

Humic acid is one of the natural organic materials (NOMs) that has been considered as one of the main contaminants in surface water. The presence of HA in water causes to produce disinfection by-products such as trihalomethanes after chlorination, unpleasant color and taste [1-4]. Consequently, it is necessary to remove them from water using effective treatment processes. Various treatment technologies including chemical coagulation/flocculation [5, 6], electrocoagulation [7-9], ultrafiltration [10-13] and adsorption [14-17] have been extensively studied for humic acid removal. Adsorption is considered as very effective, economical, versatile and simple process. Despite the expansion and application of adsorption in HA removal, difficulties in diffusion to access inner pores and separation from water solutions are still critical problems for the wider application of adsorption [18, 19]. In recent years, special attention was given to use adsorptive membranes in water treatment as a promising alternative method to solve the problem of adsorption [20, 21]. Most of these studies have mainly focused on heavy metal removal from water [21-25]. Nevertheless, there are rare reports in published literature about the application of adsorptive membranes in humic acid removal. According to Thuyavan et al. embedding

* Corresponding Author Email: *elh.shokri@bonabu.ac.ir*

of 5 wt% zirconia in polyethersulfone membrane as adsorptive membrane had 97% HA rejection [26]. Panda et al. studied HA removal by chitosan coated iron-oxide-polyacrylonitrile adsorptive membranes and evaluated their antifouling behavior. The obtained results revealed that electrostatic interaction between humic acid and positive charge of chitosan improves the HA adsorption [27].

Hence, current research has focused on developing an efficient adsorptive membrane by embedding positively charged adsorptive particles for the maximum removal of HA.

In our previous work, arginine and lysine amino acids were used as modifiers for montmorillonite (MMT) on the basis of their two positive charge chains in natural pH conditions [28]. The obtained results showed that modified MMT with arginine (MMT-A) can improve the adsorption capacity and regeneration capability of MMT for arsenic oxyanions removal. Consequently, the MMT-A was used for preparing PSf based adsorptive membranes in other studies [17, 29, 30]. The adsorption properties of modified MMT with positively charged amino acids and studies related to its applications in arsenic removal suggest that PSf/MMT-A adsorptive membranes can be useful for humic acid removal.

In order to improve the membrane performance for HA removal, the adsorption capacity of the membrane can be further improved through the use of the proper structure of polymer matrix. Studies related to the effect of membrane morphology on the behavior of adsorptive membranes have been very few. Liu et al. prepared polysulfone- graft -monoazabenzo-15-crown-5 ether adsorptive membrane for separation of lithium isotopes [31]. They found that sponge-like structure leads to an increase in contact area between adsorption sites and lithium ions. Therefore, it is necessary to enhance our understanding of the effect of membrane morphology on the adsorption behavior of membranes to extend the use of these membranes for water treatment. In this study, polyethylene glycol (PEG) is employed as an additive to control the morphology of membranes. In the following, MMT-A was embedded in PSf membranes with finger-like and sponge-like pore structures. The prepared membranes were extensively evaluated in terms of HA adsorption capacity, mechanism, kinetics, pH effect and regeneration capability. Additionally, the description of the equilibrium and kinetic data using theoretical models was carried out.

EXPERIMENTAL

Materials and methods

The polymer used as a matrix in this research was polysulfone provided by Solvay Advanced Polymer LLC. Natural montmorillonite (Cloisite Na^+) with particle size of 9-13 μm was supplied by Southern Clay Products Inc., USA. Other chemicals including N-methyl-2-pyrrolidon (NMP) (ρ: 1030 kg/m^3), PEG (M_w: 20000 g/mol), arginine, NaOH and HCl were purchased from Merck. All chemicals and reagents were analytical grades.

MMT was modified with arginine by using the method introduced in the literature [28]. Adsorptive membranes (1.5 wt% of MMT-A) were prepared by using NIPS method [29]. This amount of MMT-A was used to maximize its effect on the pure water flux and adsorption capacity of membranes, simultaneously. The composition of each casting solution and weight percentage of the casting solution is given in Table 1.

MMT-A was dissolved in NMP and sonicated for 30 min using prob sonicator (Sonopuls HD 3200, Bandelin) at room temperature. After the addition of PSf for M3 membrane and PSf-PEG for M4 membrane, the mixture was heated at 60°C for 8h. Then the resulted homogenous solution was sonicated for 15 min and then enough time was given for bubbles to be completely released. The resulted homogenous solution was cast at 150μm thickness. Immediately after casting, the film was immersed in a water bath to initiate phase inversion and then dried.

Neat membranes were prepared from a casting solution of PSf (15 wt%) with the same procedure as mentioned above without the addition of particles.

Table1. Casting solution composition of various neat and adsorptive membranes

Membrane	PSf (wt. %)	PEG (wt. %)	NMP (wt. %)	MMT-A (wt. %)
PSf (M1)	15	-	85	-
PSf/PEG (M2)	15	10	75	-
PSf/MMT-A (M3)	14.77	-	85	1.5
PSf/PEG/MMT-A (M4)	14.77	10	75	1.5

Characterization techniques

The morphology of the membranes was characterized by FE-SEM (MIRA3 FEG-SEM, Tescan). The hydrophilicity of membranes was evaluated by measuring the contact angle between the membrane surface and water droplet using a contact angle goniometer (PGX, Thwing-Albert Instrument Co.). To measure the membrane porosity, samples were cut into specific sizes before being weighed in a digital balance. The porosity of membranes was calculated using the following equation [32]:

$$\varepsilon = \frac{\left(w_w - w_d\right)/\rho_w}{\left(w_w - w_d\right)/\rho_w + \left(w_d/\rho_p\right)} \times 100 \quad (1)$$

where ε (%) is membrane porosity, w_w is the mass of wet membrane in g, w_d is the mass of dry membrane in g, ρ_w, and ρ_p are the density of isobutanol and polymer in (g/cm^3), respectively. In the determination of the porosity, the average of 3 samples of each membrane was reported.

Pure water flux of membranes was determined using a dead-end filtration system having 5cm^2 of membrane area. To minimize compaction effects, the pre-wetted membranes were compacted for 30 min at 2 bar. Then the pressure was reduced to 1.5 bar and after reaching steady state, the water flux was calculated.

The surface porosity of membranes was determined using Digimizer Image Analysis software. To determine the mean pore size of the membranes, the filtration velocity method was used following produce already established [29,30].

Adsorption experiments

Static adsorption

The static adsorption behavior of the prepared membranes was investigated with the batch experiments for humic acid solutions in the appropriate concentrations ranging from 2 to 20 ppm. For batch adsorption, adsorptive membranes (total weight 0.1g) were immersed in the HA solution (100 mL) in tap water and stirred at room temperature, while the pH of the solution was adjusted to 7.0. HA was adsorbed on the membranes thereby reducing HA concentration in the bulk until equilibrium was reached.

To determine the adsorption kinetics, the concentrations of residual HA in the prepared solutions were analyzed by UV spectrophotometer (Bio Quest CE2501) at different time intervals. The equilibrium adsorption capacity and removal efficiency of membranes were calculated as follows:

$$q_e = \frac{(C_0 - C_e)V}{M_m} \quad (2)$$

$$\%\,\mathrm{Re}moval = \frac{(C_0 - C_t)}{C_0} \times 100 \quad (3)$$

Where C_o (mg/L), C_e (mg/L) and C_t (mg/L) are concentrations at the initial, equilibrium and time t in the solution, respectively, V is the total volume (L) of the HA solution and M_m is the mass (g) of dry membrane used in the adsorption study.

To study the effect of pH on the adsorption behavior, the membranes were added into HA solutions, which were prepared at different pH (3-9). The samples were equilibrated at 25 °C in a shaking incubator and after 48 h, the concentration of HA was measured.

Continues filtration

Filtration experiments were carried out in a dead-end filtration set up with an effective surface area of 5cm^2 for membrane. The concentration of HA in the feed solution was set at 1ppm and pH of the solution was adjusted to 7.0. While 5 mL of effluent was collected at different time intervals to measure the respective HA concentrations. After saturation of membranes by HA, 50 mL NaOH solution with pH=9 filtered through the membrane. After regeneration, the second cycle of experiments was initiated and this process was repeated for five cycles.

RESULTS AND DISCUSSION

Characterization of membranes

A detailed characterization of the structural changes of MMT which take place after modification with arginine involving XRD, FTIR, zeta potential methods were reported earlier [28]. In this paper only the examination of the adsorptive membrane structure and its effect on adsorption properties were discussed.

The morphology imaging towards the surface and cross-sections of membranes can be found in Fig.1. The FE-SEM images towards the surface and cross-section of M1 and M2 membranes can be found in Fig. 1a, 1b, respectively. It can be

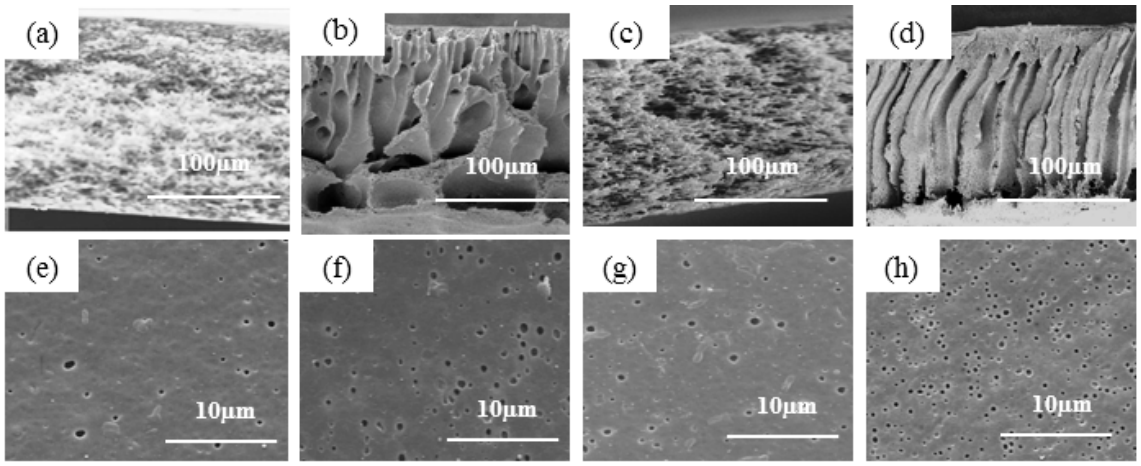

Fig. 1. FE-SEM cross-section (a–d) and top surface (e–h) images of M1 (a, e), M2 (b, f), M3 (c, g) and M4 (d, h) membranes.

Table 2. Porosity, mean pore size, surface porosity and PWF of membranes

Membrane	Porosity (%)	Mean pore size (µm)	Surface porosity (%)	PWF (Kg/m^2.h)
M1	70	0.85	15	150
M2	78	0.8	30	180
M3	74	0.8	25	160
M4	84	0.55	70	220

seen clearly that the M1 membrane has a sponge structure. In contrast to this, the M2 membrane has macrovoids which are contributed with a small tear like voids throughout. The different structure is due to PEG added to the polymer solution of the membrane. It is obvious that membrane structure in NIPS method depends on the thermodynamic equilibrium properties and transfer rates of solvent and non-solvent. The formation of macrovoids in M2 membrane is explained in terms of increase in mass ratio of non-solvent inflow and solvent outflow due to hydrophilic properties of PEG [33].

By adding MMT-A in PSf solution with PEG, macrovoids quickly transitioned into narrower voids that spanned the entire cross-section of the M4 membrane (Fig. 1d). The addition of MMT-A causes to increase the solution viscosity and can help to extend the macrovoids. In contrast, no differences in cross-sectional morphologies were observed upon MMT-A addition for the M3 membrane (Fig. 1c).

Obviously, a significant increment in surface pore sizes can be observed visually by comparing the FE-SEM top surface images of M1 (Fig. 1e); and M2 (Fig. 1f). The main reason is due to the increase in the ratio of non-solvent inflow to solvent outflow by adding PEG. The top surface images of adsorptive membranes, Fig. 1g, 1h show that the number of pores increases by incorporating MMT-A for M3 and M4.

The results of the membrane characterization in Table 2 display the porosity, mean pore size, surface porosity and the pure water flux of the prepared membranes.

As illustrated in Table 2, the porosity of the PSf membrane increases from 70 to 78% after the PEG addition and further increases to 74 and 84 for M3 and M4 membranes after embedding MMT-A, respectively. As can be seen from Table 2, embedding the MMT-A in PSf-PEG causes a decrease in the surface pore size and increase in the surface porosity significantly. The decrease of surface pore size is may be due to the increased viscosity of the solutions by embedding MMT-A [34]. However, the surface pore size and porosity values were not affected by adding PEG and MMT-A in PSf membrane.

Similar to the membrane porosity, the PWF of membranes increases by embedding MMT-A. However, a significant increase in water flux was found for the M4 membrane in comparison to the M3 membrane. These results were consistent with the observation from the FE-SEM images.

Fig. 2 depicts the water contact angle of prepared membranes. It could be found that the presence of PEG resulted in improved membrane

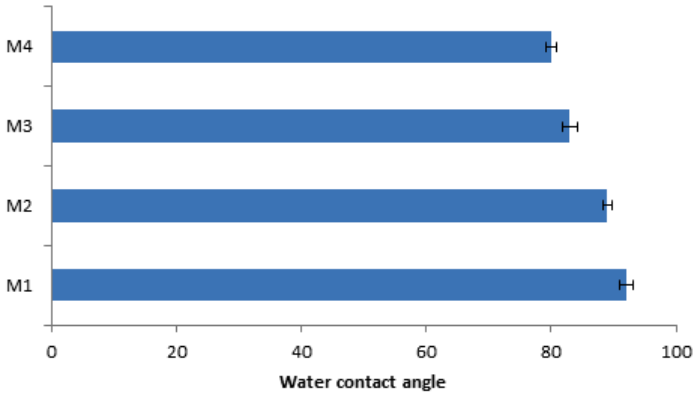

Fig. 2. Water contact angle of prepared membranes

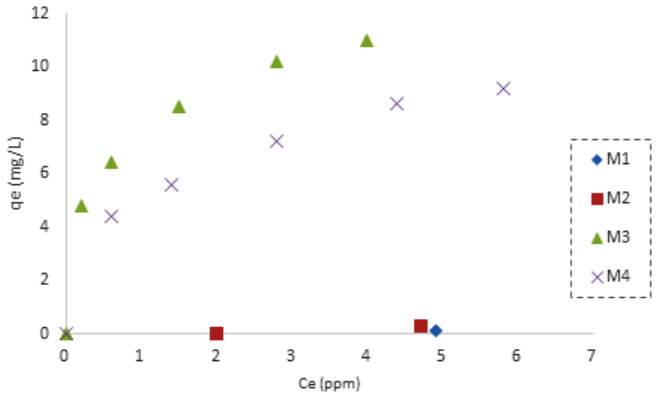

Fig. 3. The HA adsorption capacity for membranes with the different initial concentrations

hydrophilicity (lower contact angles). Furthermore, all the adsorptive membranes have less contact angle than the neat membranes because of hydrophilic polar amine functional groups of MMT-A.

Static humic acid adsorption behavior

The experimental isotherm curves of prepared membranes at different initial concentrations of HA are shown in Fig. 3. From the obtained results, it is evident that HA adsorption capacity is negligible for M1 and M2 membranes and increases as the MMT-A is embedded in the polymer solution. It is obvious that adsorption capacity increases for M3 and M4 with the increase of HA concentration. Furthermore, q_e for M3 is higher than M4, which implies that cellular structure provides effective surface area available for adsorption.

In order to understand the adsorption in more detail, Langmuir and Freundlich isotherms as two common models were used. Langmuir model assumes monolayer adsorption of adsorbate at specific homogeneous sites without any interactions among the adsorbate molecules. In contrast, Freundlich model assumes multilayer adsorption that can occur on heterogeneous surfaces. Langmuir and Freundlich models can be expressed as Eqs. (4) and (5), respectively:

$$\frac{1}{q}=\frac{1}{\left(K_L*C_e*q_{max}\right)}+\frac{1}{q_{max}} \quad (4)$$

$$\ln\left(q\right)=\ln\left(K_F\right)+\left(\frac{1}{n}\right)\ln\left(C_e\right) \quad (5)$$

Where K_L and K_F are the Langmuir and the Freundlich adsorption constants, respectively. Moreover, q_{max} is the maximal adsorption capacity and n is the heterogeneity factor.

The fitting of the Langmuir and Freundlich models to the adsorption data of HA on the M3 and M4 membranes was carried out and the results were shown in Fig. 4. The corresponding fitting parameters obtained from both Langmuir and Freundlich models were illustrated in Table 3.

According to the correlation coefficients (R^2),

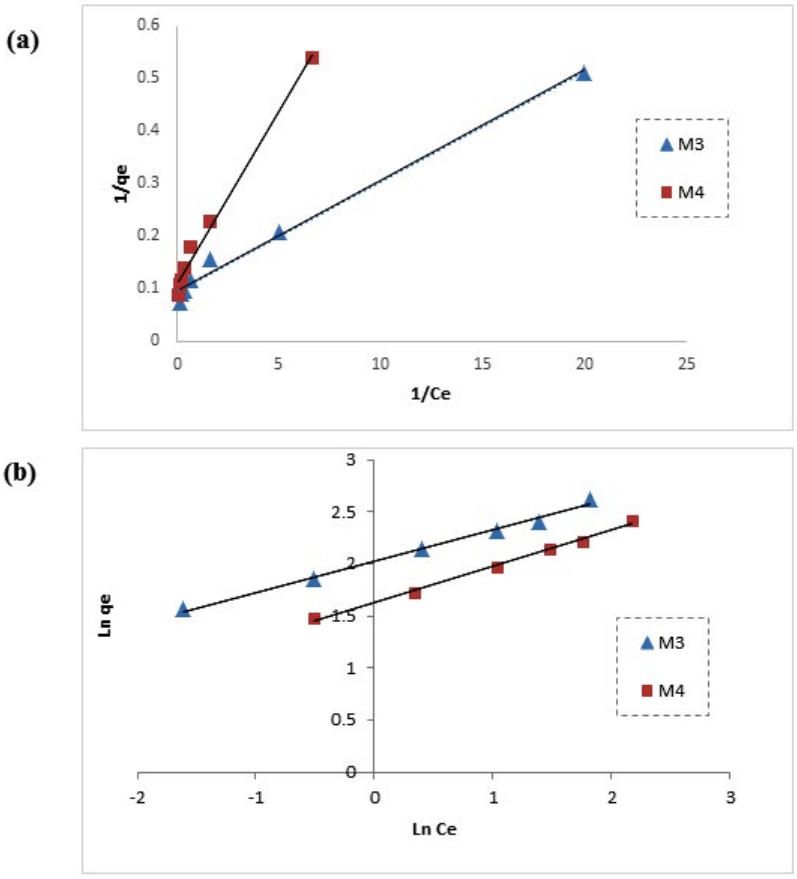

Fig. 4. Applications of adsorption isotherm models for M3 and M4 membranes with the different initial concentrations at pH = 7.0, m = 1 g/L, reaction time = 48 h, (a) Langmuir adsorption isotherm, (b) Freundlich adsorption isotherm

Table 3. Langmuir and Freundlich isotherm constants for adsorption

Membrane	Langmuir model			Freundlich model		
	q_{maX}	K_L	R^2	K_F	n	R^2
M3	10.548	4.493	0.988	5.117	2.888	0.9949
M4	9.372	1.621	0.989	7.584	3.322	0.9923

the Freundlich model describes the adsorption process better than the Langmuir model. Due to heterogeneity and complexity of the HA composition, various adsorption mechanisms can occur on adsorption sites. Ligand exchange and electrostatic attraction are proved to be main mechanism of HA adsorption on the edges of montmorillonite [2]. Moreover, electrostatic interaction between positive charge of arginine and negative charge of HA causes HA adsorption.

In order to better understand the rate of adsorption, adsorption kinetics was investigated and the effect of time on removal efficiency of M3 and M4 membranes was shown in Fig. 5.

The experimental outcomes indicate that the HA adsorption capacity increases with time. The rate of the adsorption for M3 and M4 membranes increased quickly in the first 4h and 1h, respectively and then the less marked effect was observed on increasing the contact time for both membranes.

The rapid adsorption of HA on the M4 respect to M3 may be due to the presence of large pores at the M4 membrane which facilitates the solution penetration and adsorption of HA.

In this study, the kinetics of the adsorption processes were analyzed using pseudo-first-order and pseudo-second-order equations; their mathematical equations are as below:

$$\log(q_e - q_t) = \log(q_e) - \left(\frac{k_1}{2.303}\right)t \quad (6)$$

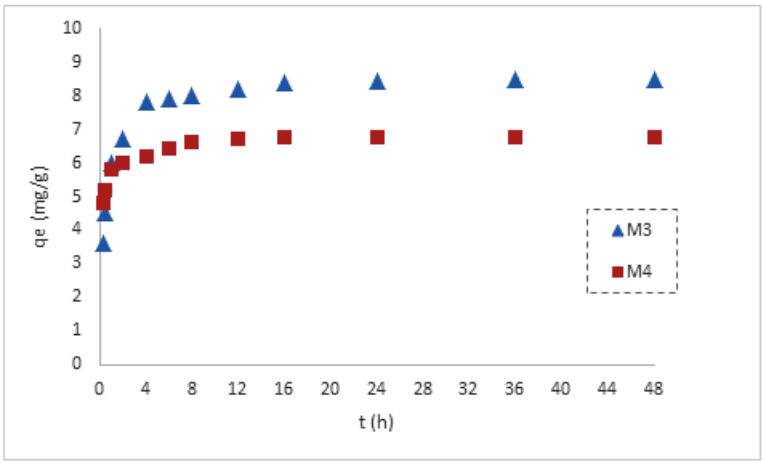

Fig. 5. The HA adsorption capacity for M3 and M4 membranes with different time intervals at pH = 7.0, m = 1 g/L, C_0=10 ppm

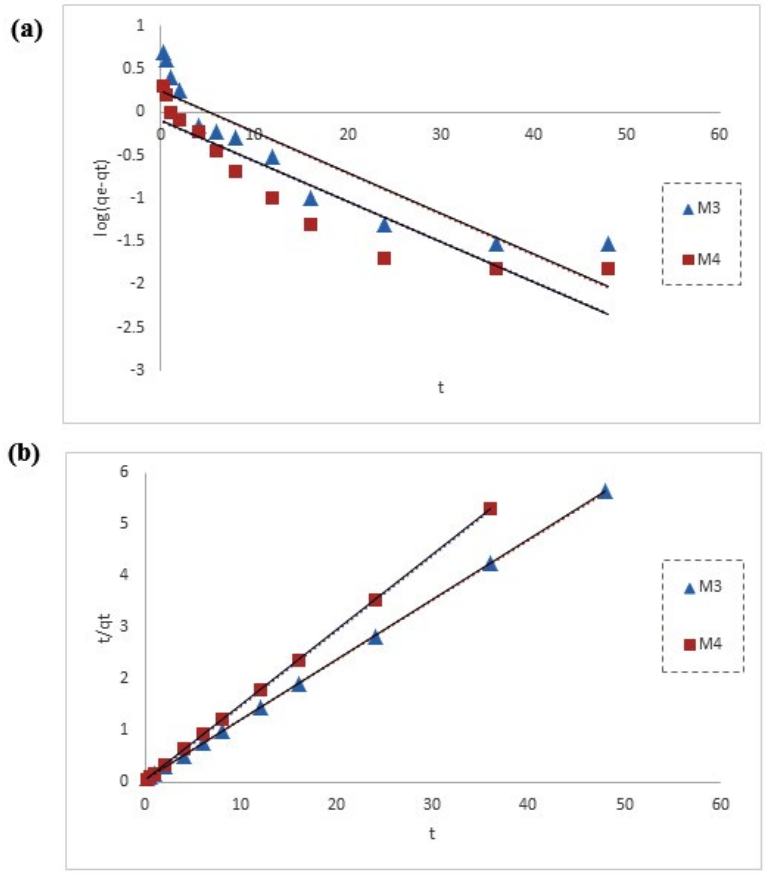

Fig. 6. Kinetic modeling of HA adsorption onto M3 and M4 membranes at pH = 7.0, m = 1 g/L, C_0=10ppm, (a), pseudo-first order adsorption kinetic model, (b), pseudo-second order adsorption kinetic model

$$\frac{t}{q_t}=\frac{1}{k_2 q_e^2}+\frac{1}{q_e}(t) \quad (7)$$

Where q_e and q_t are the amounts of HA adsorbed at equilibrium and time t (h), respectively; k_1(h^{-1}) and k_2 ($g.mg^{-1}.h^{-1}$) are the equilibrium constants of the pseudo-first-order and pseudo-second-order models, respectively.

The progress of the HA adsorption was examined by fitting the experimental data using

Table 4. The fitting parameters of adsorption kinetic model

Membrane	Pseudo-first order		Pseudo-second order			q_{actual}
	k_1	R^2	q_e	k_2	R^2	
M3	0.108	0.828	8.562	0.262	1	8.47
M4	0.109	0.828	6.831	0.612	0.999	6.78

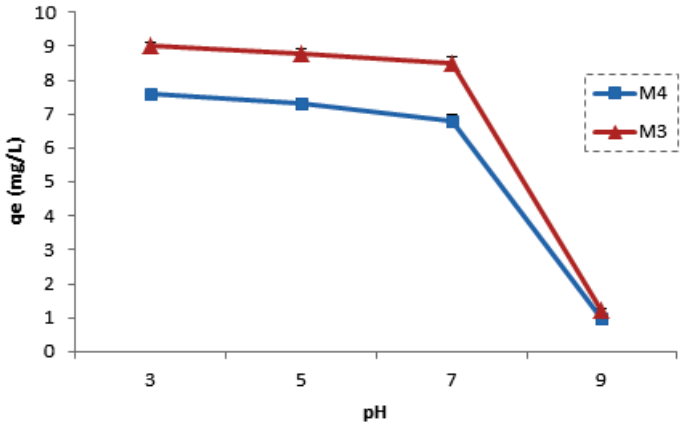

Fig. 7. The effect of solution pH on HA adsorption capacity for M3 and M4

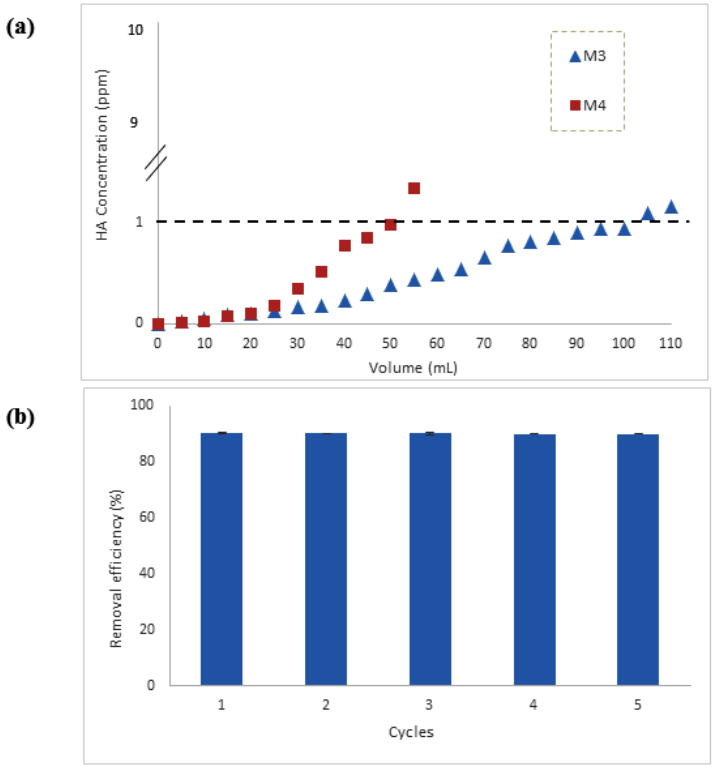

Fig.8. (a) HA concentration in the permeate as the function of volume of permeate for M3 and M4 in dynamic adsorption at C_0=10 ppm, pH=7.0, (b) Regeneration of M3 membrane at different cycles at C_0=10ppm, filtration volume=100 mL, pH=7.0

pseudo-first-order and pseudo-second-order models. As observed from Fig. 6, it is evident that R^2 for the pseudo-second-order is higher than the pseudo-first-order. Furthermore, this indicates that the adsorption is controlled by a chemisorption process. The corresponding fitting parameters for

the adsorption kinetic models from the analysis were listed in Table 4. By comparison, the values of q_e in pseudo-second order model were more in accordance with the experimental data.

The dependence of HA adsorption upon the solution pH for M3 and M4 as shown in Fig. 7. According to Fig.8, it becomes clear that HA adsorption decreases with increasing solution pH for both membranes, which can be interpreted by the surface charges of adsorptive particles embedded in membranes. The isoelectric point of MMT-A was 8 according to previous work [28]. When the pH of the solution is below 8, the surface of MMT-A has positive charge which resulted in the electrostatic attraction with negatively charged carboxyl and phenol groups of HA. It is also evident from Fig.7 that adsorption capacity of M3 is higher than M4 at all pH ranges.

Dynamic humic acid adsorption behavior

In the study of the dynamic adsorption of HA, M3 and M4 membranes were tested. Breakthrough point as the position where the concentration of pollutant rises to 10% of the feed concentration was determined for membranes. As shown in Fig. 8 (a), the M3 and M4 can effectively treat more than 100 mL and 50 mL of HA-contaminated water to ensure the HA concentration of effluents less than the MCL (1ppm), respectively. According to the results, the treatment capacity of the M3 and M4 membranes can be calculated as 200 L/m and 100 L/m, respectively. Consequently, M3 with high treatment capacity was selected for adsorption-desorption study. The reusability of M3 membrane for filtration of 100 mL HA solution (10 ppm) was investigated by running five adsorption-desorption cycles. As is apparent in Fig. 8 (b) there is low reduction in the removal efficiency of M3 even after five cycles. These results implied that M3 can be simply regenerated by treatment.

CONCLUSION

Modified montmorillonite with amino acid (MMT-A) embedded in PSf with different morphologies. The results showed that MMT-A greatly improved the hydrophilicity, permeability, and porosity of the membrane with a finger-like pore structure. No significant improvement was observed in the cellular structure membrane. Cellular membranes maintained higher HA adsorption capacity during the batch adsorption, indicating that this structure enhanced available adsorption sites. The faster HA adsorption was obtained for finger-like structure due to the presence of large pores. The cellular membrane demonstrated the highest adsorption capacity and its suitability in HA removal investigated through dead-end filtration. The obtained results suggest that this PSf adsorptive membrane with cellular structure can be effectively used to HA removal from water for multiple adsorption-desorption cycles.

CONFLICTS OF INTEREST

There are no conflicts to declare.

REFERENCES

1. Sutzkover-Gutman I, Hasson D, Semiat R. Humic substances fouling in ultrafiltration processes. Desalination. 2010;261(3):218-31.
2. Derakhshani E, Naghizadeh A. Optimization of humic acid removal by adsorption onto bentonite and montmorillonite nanoparticles. Journal of Molecular Liquids. 2018;259:76-81.
3. Erhayem M, Sohn M. Effect of humic acid source on humic acid adsorption onto titanium dioxide nanoparticles. Science of The Total Environment. 2014;470-471:92-8.
4. Domany Z, Galambos I, Vatai G, Bekassy-Molnar E. Humic substances removal from drinking water by membrane filtration. Desalination. 2002;145(1-3):333-7.
5. Deng L, Ngo H-H, Guo W, Zhang H. Pre-coagulation coupled with sponge-membrane filtration for organic matter removal and membrane fouling control during drinking water treatment. Water Research. 2019;157:155-66.
6. Ma B, Xue W, Hu C, Liu H, Qu J, Li L. Characteristics of microplastic removal via coagulation and ultrafiltration during drinking water treatment. Chemical Engineering Journal. 2019;359:159-67.
7. Kac FU, Kobya M, Gengec E. Removal of humic acid by fixed-bed electrocoagulation reactor: Studies on modelling, adsorption kinetics and HPSEC analyses. Journal of Electroanalytical Chemistry. 2017;804:199-211.
8. Feng Q-y, Li X-d, Cheng Y-j, Meng L, Meng Q-j. Removal of Humic Acid from Groundwater by Electrocoagulation. Journal of China University of Mining and Technology. 2007;17(4):513-20.
9. Kuokkanen V, Kuokkanen T, Rämö J, Lassi U. Electrocoagulation treatment of peat bog drainage water containing humic substances. Water Research. 2015;79:79-87.
10. Xia S, Ni M. Preparation of poly(vinylidene fluoride) membranes with graphene oxide addition for natural organic matter removal. Journal of Membrane Science. 2015;473:54-62.
11. Kanagaraj P, Nagendran A, Rana D, Matsuura T. Separation of macromolecular proteins and removal of humic acid by cellulose acetate modified UF membranes. International Journal of Biological Macromolecules. 2016;89:81-8.
12. Rao G, Zhang Q, Zhao H, Chen J, Li Y. Novel titanium dioxide/iron (III) oxide/graphene oxide photocatalytic membrane for enhanced humic acid removal from water. Chemical Engineering Journal. 2016;302:633-40.

13. Vatanpour V, Shockravi A, Zarrabi H, Nikjavan Z, Javadi A. Fabrication and characterization of anti-fouling and anti-bacterial Ag-loaded graphene oxide/polyethersulfone mixed matrix membrane. Journal of Industrial and Engineering Chemistry. 2015;30:342-52.
14. Iqbal J, Shah NS, Sayed M, Imran M, Muhammad N, Howari FM, et al. Synergistic effects of activated carbon and nano-zerovalent copper on the performance of hydroxyapatite-alginate beads for the removal of As3+ from aqueous solution. Journal of Cleaner Production. 2019;235:875-86.
15. Li L, Iqbal J, Zhu Y, Zhang P, Chen W, Bhatnagar A, et al. Chitosan/Ag-hydroxyapatite nanocomposite beads as a potential adsorbent for the efficient removal of toxic aquatic pollutants. International Journal of Biological Macromolecules. 2018;120:1752-9.
16. Tang Y, Liang S, Yu S, Gao N, Zhang J, Guo H, et al. Enhanced adsorption of humic acid on amine functionalized magnetic mesoporous composite microspheres. Colloids and Surfaces A: Physicochemical and Engineering Aspects. 2012;406:61-7.
17. Zheng Y-M, Zou S-W, Nanayakkara KGN, Matsuura T, Chen JP. Adsorptive removal of arsenic from aqueous solution by a PVDF/zirconia blend flat sheet membrane. Journal of Membrane Science. 2011;374(1-2):1-11.
18. He J, Cui A, Ni F, Deng S, Shen F, Song C, et al. In situ-generated yttrium-based nanoparticle/polyethersulfone composite adsorptive membranes: Development, characterization, and membrane formation mechanism. Journal of Colloid and Interface Science. 2019;536:710-21.
19. Guo Y, Jia Z. Novel sandwich structure adsorptive membranes for removal of 4-nitrotoluene from water. Journal of Hazardous Materials. 2016;317:295-302.
20. Abdullah N, Gohari RJ, Yusof N, Ismail AF, Juhana J, Lau WJ, et al. Polysulfone/hydrous ferric oxide ultrafiltration mixed matrix membrane: Preparation, characterization and its adsorptive removal of lead (II) from aqueous solution. Chemical Engineering Journal. 2016;289:28-37.
21. Sahebjamee N, Soltanieh M, Mousavi SM, Heydarinasab A. Removal of Cu2+, Cd2+ and Ni2+ ions from aqueous solution using a novel chitosan/polyvinyl alcohol adsorptive membrane. Carbohydrate Polymers. 2019;210:264-73.
22. Ahmadzadeh Tofighy M, Mohammadi T. Nickel ions removal from water by two different morphologies of induced CNTs in mullite pore channels as adsorptive membrane. Ceramics International. 2015;41(4):5464-72.
23. Salehi E, Madaeni SS, Rajabi L, Derakhshan AA, Daraei S, Vatanpour V. Static and dynamic adsorption of copper ions on chitosan/polyvinyl alcohol thin adsorptive membranes: Combined effect of polyethylene glycol and aminated multi-walled carbon nanotubes. Chemical Engineering Journal. 2013;215-216:791-801.
24. Salehi E, Madaeni SS, Rajabi L, Vatanpour V, Derakhshan AA, Zinadini S, et al. Novel chitosan/poly(vinyl) alcohol thin adsorptive membranes modified with amino functionalized multi-walled carbon nanotubes for Cu(II) removal from water: Preparation, characterization, adsorption kinetics and thermodynamics. Separation and Purification Technology. 2012;89:309-19.
25. Thuyavan YL, Anantharaman N, Arthanareeswaran G, Ismail AF. Adsorptive Removal of Humic Acid by Zirconia Embedded in a Poly(ether sulfone) Membrane. Industrial & Engineering Chemistry Research. 2014;53(28):11355-64.
26. Panda SR, Mukherjee M, De S. Preparation, characterization and humic acid removal capacity of chitosan coated iron-oxide- polyacrylonitrile mixed matrix membrane. Journal of Water Process Engineering. 2015;6:93-104.
27. Shokri E, Yegani R, Pourabbas B, Ghofrani B. Evaluation of modified montmorillonite with di-cationic surfactants as efficient and environmentally friendly adsorbents for arsenic removal from contaminated water. Water Science and Technology: Water Supply. 2017;18(2):460-72.
28. Shokri E, Yegani R, Akbarzadeh A. Novel adsorptive mixed matrix membranes by embedding modified montmorillonite with arginine amino acid into polysulfones for As(V) removal. Applied Clay Science. 2017;144:141-9.
29. Shokri E, Yegani R, Pourabbas B, Kazemian N. Preparation and characterization of polysulfone/organoclay adsorptive nanocomposite membrane for arsenic removal from contaminated water. Applied Clay Science. 2016;132-133:611-20.
30. Liu Y, Yan F, Pei H, Li J, Cui Z, He B, et al. Preparation of PSf-g-BN15C5/NWF composite membrane with sponge-like pore structure for lithium isotopes adsorptive separation. Journal of the Taiwan Institute of Chemical Engineers. 2018;91:507-16.
31. Yegani. Full-Factorial Experimental Design to Determine the Impacts of Influential Parameters on the Porosity and Mechanical Strength of LLDEP Microporous Membrane Fabricated via Thermally Induced Phase Separation Method. Journal of Membrane and Separation Technology. 2012.
33. Kim, J.H. and K.H. Lee, *Effect of PEG additive on membrane formation by phase inversion* Joum0a of Membrane Science 1998. **138**: p. 153-163.
33. Vatanpour V, Madaeni SS, Rajabi L, Zinadini S, Derakhshan AA. Boehmite nanoparticles as a new nanofiller for preparation of antifouling mixed matrix membranes. Journal of Membrane Science. 2012;401-402:132-43.